Removal of defects in a colloidal crystal grown in an inverted pyramidal container by changing the external force

doi: 10.7567/JJAP.54.110301

Removal of defects in a colloidal crystal grown in an inverted pyramidal container by changing the external force

Youhei Kanatsu[1] and Masahide Sato[2]

[1] *Graduate School of Natural Science and Technology, Kanazawa University, Kanazawa 920-1192, Japan*
[2] *Information Media Center, Kanazawa University, Kanazawa 920-1192, Japan*

Keeping the formation of colloidal crystals by sedimentation in mind, we carry out Brownian dynamics simulations and study the crystallization of colloidal particles in an inverted pyramidal container. When an external force is added, the sedimentation of particles occurs and the particle density increases in the low region of the inverted pyramidal container. The crystallization of particles occurs and the face-centered cubic structure is formed in the container. When the force is large, the particles with the hexagonal close-packed structure and disordered particles are also formed and act as defects in bulk. After the sedimentation finishes, we decrease the force transiently. The defects in bulk are removed from the bulk.

A close-packed colloidal crystal with the face-centered cubic (fcc) structure is considered as a coordinate of an inverted opal with a three-dimensional full photonic band gap,[1)] and the sedimentation of colloidal particles[2)] is a useful method to form close-packed colloidal crystals. During sedimentation, particles form a triangular lattice when they deposit on the flat bottom. The lattice acts as the {111} face of the fcc structure and the growth of grains with the fcc structure occurs. However, there are two stacking ways on the triangular lattice. Thus, grains with the hexagonal close-packed (hcp) structure can also grow on the lattice[2,3)] although the fcc structure is more stable than the hcp structure.[4,5)]

To prevent the formation of grains with the hcp structure, Matsuo *et al.* used an inverted pyramidal pit[6)] as a container. When the inclination of the pyramidal surfaces of the pit is suitable and the direction of an external force inducing the sedimentation is parallel to the central axis, the triangular lattice is formed on the pyramidal surfaces and the growing interface, which is perpendicular to the external force, becomes the {100} face of the fcc structure. Since the stacking way is unique on the {100} face, the crystal with the fcc structure grows without forming the grains with the hcp structure. Keeping the experiment of Matsuo *et al.*[6)] in mind, we have carried out

Brownian dynamics simulations[7] in which the sedimentation of particles induced by an external force occurs in an inverted pyramidal container. When the inclination of the pyramidal surfaces of the container is suitable, large grains with the fcc structure are formed in the container, which agrees with the experiment of Matsuo *et al.*[6] When the force is small, the number of disordered particles in bulk is small, but the growth rate of crystal is low and many liquidlike particles remain in the upper region. On the other hand, the crystallization proceeds fast and almost all the particles are solidified with a strong force. However, many defects, which are formed by the disordered and hcp structured particles, remain in the bulk. Rapid crystal formation is an advantage when we use colloidal crystals as materials of devices, but removing the disordered particles from rapid grown crystals is necessary. Thus, in this study, by carrying out Brownian dynamics simulations, we examine the possibility of removing the defects from rapidly grown colloidal crystals by transiently decreasing the force.

We use a standard and simple model, which we used in our previous studies.[7–12] We consider that particles receive a strong frictional force proportional to their velocity. The equation of motion of the ith particle is given by

$$\frac{\mathrm{d}\boldsymbol{r}_i}{\mathrm{d}t} = \frac{1}{\zeta}\left(F_{\mathrm{ext}}\mathbf{e}_{\mathrm{ext}} - \sum_{i\neq j}\boldsymbol{\nabla}U(r_{ij}) + \boldsymbol{F}_i^{\mathrm{B}}\right), \tag{1}$$

where ζ is the frictional coefficient and $\boldsymbol{r}_i$ is the position of the ith particle. $\boldsymbol{F}_{\mathrm{ext}}$ is the external force causing the sedimentation. The second term represents the force induced by the interaction between particles. In the experiment by Matsuo *et al.*,[6] the interaction is probably a short-range repulsion. Thus, for simplicity we use the Weeks–Chandler–Anderson (WCA) potential[13] as the interaction potential. The WCA potential between the ith and jth particles is given by

$$U(r_{ij}) = \begin{cases} 4\epsilon\left[\left(\dfrac{\sigma}{r_{ij}}\right)^{12} - \left(\dfrac{\sigma}{r_{ij}}\right)^{6} + \dfrac{1}{4}\right] & (r_{ij} \leq r_{\mathrm{in}}), \\ 0 & (r_{ij} \geq r_{\mathrm{in}}), \end{cases} \tag{2}$$

where σ represents the diameter of particles, $r_{ij} = |\boldsymbol{r}_i - \boldsymbol{r}_j|$ is the distance between the ith and jth particles, and $r_{\mathrm{in}} = 2^{1/6}\sigma$. In the equation of motion, $\boldsymbol{F}_i^{\mathrm{B}}$ represents the isotropic random force. Its average is 0 and the time correlation is given by

$$\left\langle F_{m,i}^{\mathrm{B}}(t)F_{n,i}^{\mathrm{B}}(t')\right\rangle = 2\zeta k_{\mathrm{B}}T\delta_{mn}\delta_{ij}\delta(t-t'), \tag{3}$$

where $F_{m,i}^{\mathrm{B}}(t)$ represents the random force component in the mth direction for the ith

particle at time t. A simple difference equation is given by [14)]

$$\tilde{\boldsymbol{r}}_i(\tilde{t}+\Delta\tilde{t}) = \tilde{\boldsymbol{r}}_i(\tilde{t}) + [\tilde{\boldsymbol{F}}_{\rm ext} - \sum_{i\neq j} \boldsymbol{\nabla} U(\tilde{r}_{ij})]\Delta\tilde{t} + \Delta\tilde{\boldsymbol{r}}_i^{\rm B}, \tag{4}$$

where $\tilde{\boldsymbol{r}}_i = \boldsymbol{r}_i/\sigma$ $\tilde{t} = t\epsilon/\zeta\sigma^2$, and $\tilde{\boldsymbol{F}}_{\rm ext} = \tilde{\boldsymbol{F}}_{\rm ext}\sigma/\epsilon$, respectively. The last term $\Delta\tilde{\boldsymbol{r}}_i^{\rm B}$ represents the normalized isotropic displacement by a random force. The displacement satisfies $\left\langle \Delta\tilde{r}_{m,i}^{\rm B}(\tilde{t})\Delta\tilde{r}_{n,i}^{\rm B}(\tilde{t}')\right\rangle = 2\tilde{R}^{\rm B}\Delta\tilde{t}\delta_{m,n}\delta_{ij}\delta(\tilde{t}-\tilde{t}')$, where $\Delta r_{m,i}^{\rm B}(t)$ represents the random displacement component in the m direction for the ith particle and $\tilde{R}^{\rm B} = k_{\rm B}T/\epsilon$.

To determine the property of the the connection between the ith and jth particles, we introduce $d_l(i,j)$, which is defined as[15,16)]

$$d_l(i,j) = \sum_{m=-l}^{l} q_{l,m}(i)q_{l,m}^*(j), \tag{5}$$

where

$$q_{l,m}(i) = \frac{1}{n_{\rm n}}\sum_{j=1}^{n_{\rm n}} Y_l^m(\theta_{ij},\phi_{ij}), \tag{6}$$

and $q_{l,m}^*(j)$ is the complex conjugate of $q_{l,m}(j)$. In Eq. (6), $n_{\rm n}$ is the number of neighboring particles, θ_{ij} is the polar angle, ϕ_{ij} is the azimuthal angle, and $Y_l^m(\theta_{ij},\phi_{ij})$ is the spherical harmonics. The repulsion between the two particles occurs when $r_{ij} < r_{\rm in}$. Thus, taking account of random displacement, we regard the two particles as neighbors if $r_{ij} < 1.1r_{\rm in}$. We consider that the connection between the ith and jth particles is solidlike when $d_6(i,j) > 0.7$. If the number of solidlike connections is 4 or more, the ith particle is regarded as a solidlike particle. In our simulation, the hcp and fcc structures are formed as the close-packed structures. To distinguish the two structures, we use $Q_l(i)$ and $w_l(i)$[17–21)]. The two order parameters are defined as

$$Q_l(i) = \sqrt{\alpha_l \sum_{m=-l}^{l} |q_{l,m}(i)|^2}, \tag{7}$$

$$w_l(i) = \sum_{m_1,m_2,m_3} \begin{pmatrix} l & l & l \\ m_1 & m_2 & m_3 \end{pmatrix} \times \alpha_l^{3/2} \frac{q_{l,m_1}(i)q_{l,m_2}(i)q_{l,m_3}(i)}{Q_l(i)^3}, \tag{8}$$

where $\alpha_l = 4\pi/(2l+1)$. The integers m_1, m_2, and m_3 satisfy $-l \le m_1, m_2, m_3 \le l$ and $m_1 + m_2 + m_3 = 0$. The term in parentheses in Eq. (8) is the Wigner 3-j symbol. We may not be able to determine the local structure correctly if $n_{\rm n}$ is small. Thus, we do not determine the local structure around the particle when $n_{\rm n} \le 9$ and regard it as

a disordered solidlike particle. We calculate $Q_l(i)$ and $w_l(i)$ and determine the local structure when a solidlike particle has 10 or more neighbors. If $-0.18 < w_4(i) < -0.01$ and $0.175 < Q_4(i) < 0.2$, we consider the local structure around the ith particle as the fcc structure. If $0.02 < w_4(i) < 0.15$ and $0.06 < Q_4(i) < 0.15$, we regard the local structure around the ith particle as the hcp structure. The criteria are the same as those used in previous studies.[7,10–12)]

We carry out simulations in an inverted pyramidal container.[7)] The positions of the four corners in the base of the pyramidal container are given by $\mathrm{A}(\tilde{L}, 0, \tilde{L})$, $\mathrm{B}(0, \tilde{L}, \tilde{L})$, $\mathrm{C}(-\tilde{L}, 0, \tilde{L})$, and $\mathrm{D}(0, -\tilde{L}, \tilde{L})$, and the apex position is given by $\mathrm{O}(0, 0, 0)$. The particle number N and the volume fraction ϕ are set to be 23328 and 0.1, respectively. $\tilde{L} = (2\pi N/\phi)^{1/3}\sigma$, $\tilde{R}_B = 0.1$, and $\Delta\tilde{t} < 10^{-3}$. Initially, we put the particles in the container at random. To eliminate the effect of the initial positions, we move the particles without adding an external force. Then, we add $\tilde{\boldsymbol{F}}_{\mathrm{ext}} = \tilde{F}_{\mathrm{ext}}(0, 0, -1)$ and start the sedimentation. The force strength $\tilde{F}_{\mathrm{ext}} = \tilde{F}_{\mathrm{max}}$ in the first stage. Then, $\tilde{F}_{\mathrm{ext}}$ is suddenly decreased and kept at F_{min} temporarily in the second stage. In the third stage, $\tilde{F}_{\mathrm{ext}}$ is returned to $\tilde{F}_{\mathrm{max}}$ and maintained at this value. We carry out simulation, setting $\tilde{F}_{\mathrm{max}} = 1$.

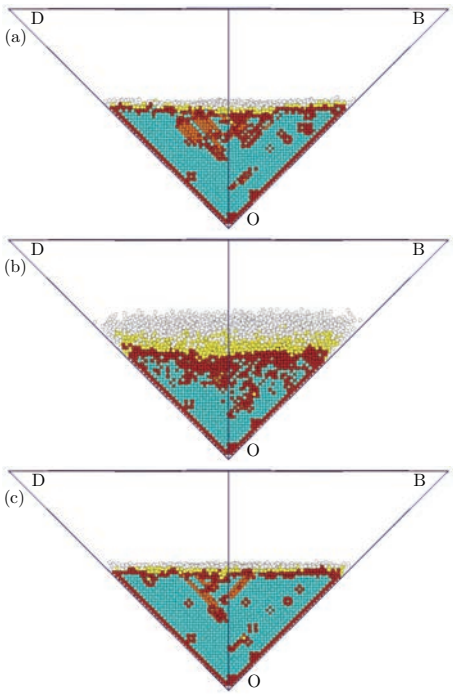

Fig. 1. (color online) Snapshots in bulk in the (a) first ($\tilde{t} = 300$), (b) second ($\tilde{t} = 384$), and (c) third ($\tilde{t} = 500$) stages. $\tilde{F}_{\mathrm{max}} = 1.0$ and $\tilde{F}_{\mathrm{min}} = 0.2$

We cut the container along the plane OBD and examine the bulk structure. Figure 1 shows the snapshots in each stage. We color the particles to distinguish their states. White (the brightest) and yellow particles (the second brigthest) are dilute liquidlike particles and dense liquidlike particles, respectively. Red (the darkest) particles are disordered solidlike particles, whose local structure we cannot determine. Blue (the third darkest) and orange (the second darkest) particles represent the fcc structured particles and the hcp structured particles, respectively. In the initial stage [Fig. 1(a)], almost all the particles seem to have the fcc structure although there are a few disordered particles and hcp structured particles in the bulk. Thin layers of the liquidlike particles are formed on the top of the solidlike particles. In sedimentation, the strength of the external force to the thermal diffusion is expressed by the Peclet number Pe, which is given by $Pe = F_{\rm ext}\sigma/2k_{\rm B}T = \tilde{F}_{\rm ext}/2\tilde{R}_{\rm B}$. When $\tilde{F}_{\rm ext} = 1.0$, Pe is probably much larger than that obtained by Matsuo *et al.*,[6] as estimated in our previous study.[7] Thus, the disordered solidlike particles remain in the bulk although the system is not very large in our simulations. In the second stage [Fig. 1(b)], the solidlike particles in the upper region melt and the width of the layers of liquidlike particles increases. The hcp structured particles in the upper central region change to the disordered solidlike particles or liquidlike particles. In the lower region, some fcc structured particles around disordered particles change to the disordered particles. Thus, not only near the interface but also in the low region, the particles are affected by the decrease in the external force. In the third stage [Fig. 1(c)], the particles in the upper region are solidified again. By comparing Fig. 1(a) with Fig. 1(c), we find that some hcp structured particles and disordered solidlike particles change to the fcc structured particles.

Figure 2 shows the time evolution of the numbers of the ordered particles, in which $N_{\rm fcc}$ and $N_{\rm hcp}$ represent the numbers of the fcc and hcp structures, respectively. $\tilde{F}_{\rm ext}$ changes from $\tilde{F}_{\rm max}$ to $\tilde{F}_{\rm min}$ at $\tilde{t} = 300$ and returns to $\tilde{F}_{\rm max}$ at $\tilde{t} = 400$. In the fist stage ($0 < \tilde{t} < 300$), both $N_{\rm fcc}$ and $N_{\rm hcp}$ increase with increasing time and saturate at $\tilde{t} = 200$. $N_{\rm fcc}$ is much larger than $N_{\rm hcp}$. In the second stage ($300 < \tilde{t} < 400$), $N_{\rm fcc}$ and $N_{\rm hcp}$ decrease and reach their minimum at $t \simeq 330$. In the third stage ($400 < \tilde{t} < 600$), in which the force strength is the same as that in the first stage, $N_{\rm fcc}$ and $N_{\rm hcp}$ increase and immediately saturates. Compared with the case in which the force is kept at $F_{\rm max}$, $N_{\rm fcc}$ slightly increases owing to the temporary decrease in $\tilde{F}_{\rm ext}$.

Figure 3 shows the distributions of the particle densities in the three stages. We slice the pyramidal container into layers of thin truncated square pyramids with a

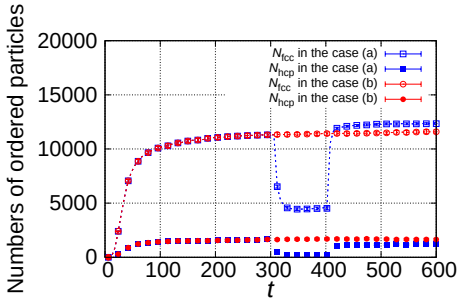

Fig. 2. (color online) Time evolution of the number of fcc structured particles ($N_{\rm fcc}$) and that of hcp structured particles ($N_{\rm hcp}$). In the case of (a), $\tilde{F}_{\rm ext}$ remains at 1.0. In the case of (b), $\tilde{F}_{\rm ext}$ changes from $\tilde{F}_{\rm max}$ to $\tilde{F}_{\rm min}$ at $\tilde{t} = 300$ and returned to $\tilde{F}_{\rm max}$ at $\tilde{t} = 400$, in which $\tilde{F}_{\rm max} = 1.0$ and $\tilde{F}_{\rm min} = 0.2$. The data are averages of 10 samples.

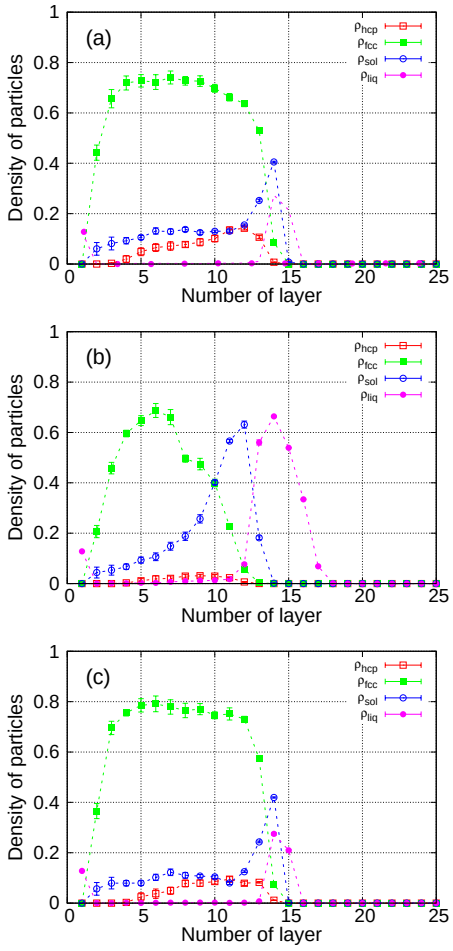

Fig. 3. (color online) Distribution of particle densities in the (a) first ($t = 300$), (b) second ($t = 384$), and (c) third ($t = 600$) stages. $\rho_{\rm fcc}$, $\rho_{\rm hcp}$, $\rho_{\rm sol}$, and $\rho_{\rm liq}$ represent the densities of fcc structured particles, hcp structured particles, disordered solidlike particles, and liquidlike particles, respectively. The data are averages of 10 samples.

small width, $\tilde{L}/25$, along the z-axis. In Fig. 3, the number of layers increases with increasing height. We count the particle numbers and calculate the particle densities in each layer. The particles attaching to the pyramidal surfaces of the container are not counted, so that the sum of the densities is small near the origin. Figure 3(a) shows the density distributions in the first stage. In the low region, the density of the fcc structured particles, $\rho_{\rm fcc}$, is much higher than those of the disordered and hcp structured particles, $\rho_{\rm sol}$ and $\rho_{\rm hcp}$, respectively. The density of the liquidlike particles $\rho_{\rm liq} \simeq 0$. With increasing the height, $\rho_{\rm sol}$ and $\rho_{\rm hcp}$ increase and $\rho_{\rm fcc}$ decreases. Here, we define the interface position as the height at which $\rho_{\rm liq}$ is larger than $\rho_{\rm sol}$. The interface position is in the 15th layer. Figure 3(b) shows the distribution of particles in the second stage. In the upper region, the densities of disordered solidlike and liquidlike particles increase after melting. $\rho_{\rm fcc}$ decreases largely between the second layer to the 12th layer. The interface position falls to the 13th layer. In the third stage [Fig. 3(c)], the interface position returns to the 15th layer, which is the same as that before decreasing $F_{\rm ext}$. The densities $\rho_{\rm sol}$, $\rho_{\rm liq}$, $\rho_{\rm hcp}$, and $\rho_{\rm fcc}$ change from those in Fig. 3(a). However, the differences in the densities are small. Thus, in Fig. 4 we show the density differences. The density distribution

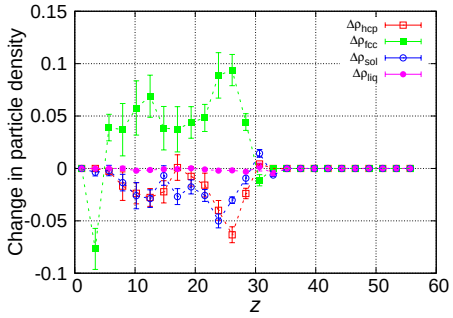

Fig. 4. (color online) Changes in particle densities induced by the temporary decrease in force. The data are averages of 10 samples.

of the liquidlike particles hardly changes, but the densities of the hcp structure and disordered solidlike particles decrease and that of the fcc structured particles increases. The increase in the density of fcc structured particles occurs in the low region, but the change in the density is smaller than that in the upper region.

Finally, we change $\tilde{F}_{\rm min}$ and investigate how $N_{\rm fcc}$ and $N_{\rm hcp}$ change with $\Delta\tilde{F}_{\rm ext} = \tilde{F}_{\rm max} - \tilde{F}_{\rm min}$. Figure 5(a) shows the dependence of $N_{\rm fcc}$ on $\Delta\tilde{F}_{\rm ext}$. When $\Delta\tilde{F}_{\rm ext}$ is small, $N_{\rm fcc}$ increases with increasing $\Delta\tilde{F}_{\rm ext}$ because the rearrangement of the particle positions

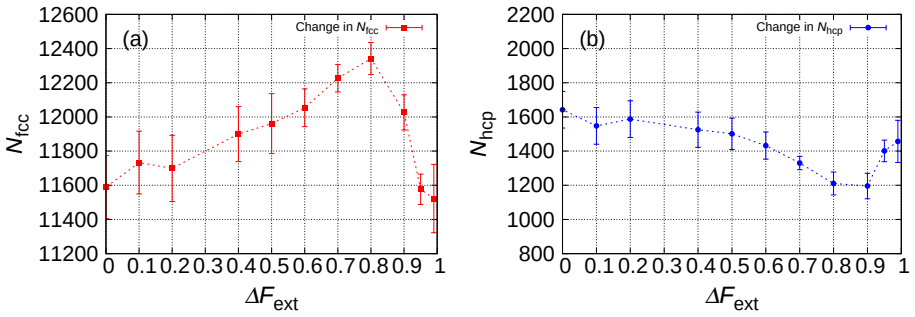

Fig. 5. (color online) Dependences of (a) $N_{\rm hcp}$ and (b) $N_{\rm fcc}$ on the decrease in the external force, $\Delta\tilde{F}_{\rm ext}$. The data are averages of 10 samples.

occurs more widely with increasing $\Delta\tilde{F}_{\rm ext}$. On the other hand, $N_{\rm fcc}$ decreases with increasing $\Delta\tilde{F}_{\rm ext}$ when $\Delta\tilde{F}_{\rm ext} > 0.8$. During recrystallization of the melted particles in the third stage, the unmelted fcc structured particles act as the substrate. When $\Delta\tilde{F}_{\rm ext}$ is too large, many fcc structured particles melt and the density of particles acting as the substrate decreases. The sedimentation of particles on the suitable positions becomes difficult: thus, the disordered solidlike and hcp structured particles remain in the bulk. In Fig. 5(b), we show the dependence of $N_{\rm hcp}$ on $\Delta\tilde{F}_{\rm ext}$, which is the opposite to that of $N_{\rm fcc}$. The change in $N_{\rm hcp}$ is smaller than that in $N_{\rm fcc}$ because the disordered particles also changes to the fcc structured particles owing the temporary force decrease.

In this study, keeping a colloidal crystal formed by sedimentation in mind, we carried our Brownian dynamics simulations. We studied how defects decrease with the temporary decrease in force. When the force is decreased temporarily, the disordered solidlike particles melt near the interface. When the force is increased again, the melted particles move to the suitable positions and the ordering is improved by recrystallization. In the low region, the pressure originating from the upper particles decreases. Thus, although the decrease in pressure is smaller than that near the interface, the particles can move and rearrangement of the disordered particles occurs. However, when the decrease in $\tilde{F}_{\rm ext}$ is too large, the fcc structured particles acting as the substrate melt. Since the advantage of the recrystallization is lost, $N_{\rm fcc}$ decreases with increasing force in the region with large $\tilde{F}_{\rm ext}$.

When the sedimentation of the polystyrene particles with the diameter $\sigma = 1.0$ μm occurs in water owing to the gravitational force, the Peclet number is estimated to be $Pe = 3.6 \times 10^{-2}$. This estimated Pe is much smaller than that obtained by our simulation. However, if the sedimentation is carried out with centrifugal force,[22] a

large Pe number is obtained. Thus, the removal of defects by controlling the external force probably occurs when an experiment is carried out under centrifugal force.

Mori et al.[23] carried out Monte Carlo simulation and showed that grains become large with a stepwise increase in force. If we grow crystal by changing $\tilde{F}_{\rm ext}$ in an early stage, the formation of defects in the lower region may be prevented. In the future, we will study the effects of the time profile of force on the structure in the bulk.

Acknowledgements This work was supported by JSPS KAKENHI Grants Nos. 26103515 and 26390054. M.S. benefited from the Joint Research Program of the Institute of Low Temperature Science, Hokkaido University.

References

1) A. Blanco, E. Chomski, S. Grabtchak, M. Ibisate, S. John, S. W. Leonard, C. Lopez, F. Meseguer, H. Miguez, J. P. Mondia, G. A. Ozin, O. Toader, and H. M. Van Diel, Nature **405**, 437 (2000).
2) J. Zhu, M. Li, R. Rogers, W. Meyer, R. H. Ottewill, STS-73 Space Shuttle Crew, W. B. Russel, and P. M. Chaikin, Nature **387**, 883 (1997).
3) P. N. Pusey, W. V. Megen, P. Bartlett, B. J. Ackerson, J. G. Rarity, and S. M. Underwood, Phys. Rev. Lett. **63**, 2753 (1989).
4) L. V. Woodcok, Nature **385**, 141 (1997)
5) H. Míguez, F. Meseguer, C. López, A. Mifsud, J. S. Moya, and L. Vázquez, Lagnumuir **13**, 6009 (1997).
6) S. Matsuo, T. Fujine, K. Fukuda, S. Juodkazis, and H. Misawa, Appl. Phys. Lett. **82**, 4285 (2003).
7) Y. Kanatsu and M. Sato, J. Phys. Soc. Jpn. **84**, 044601 (2015).
8) M. Sato, H. Katsuno, and Y. Suzuki, Phys. Rev. E **87**, 032403 (2013).
9) M. Sato, H. Katsuno, and Y. Suzuki, J. Phys. Soc. Jpn. **82**, 084804 (2013).
10) M. Sato, Y. Suzuki, and H. Katsuno, J. Cryst. Growth **401**, 87 (2014).
11) M. Fujine, M. Sato, H. Katsuno, and Y. Suzuki, Phys. Rev. E **89**, 042401 (2014).
12) M. Fujine, M. Sato, T. Toyooka, H. Katsuno, and Y. Suzuki, and T. Sawada, Phys. Rev. E **90**, 032404 (2014).
13) J. D. Weeks, D. Chandler, and H. C. Anderson, J. Chem. Phys. **54**, 5237 (1971).
14) D. L. Ermak, J. Chem. Phys. **62**, 4189 (1975).
15) P. R. ten Wolde, M. J. Ruiz-Montero, and D. Frenkel, Phys. Rev. Lett **75**, 2714 (1995).
16) M. Marechal, M. Hermes, and M. Dijkstra, J. Chem. Phys. **135**, 034510 (2011).
17) P. J. Steinhardt, D. R. Nelson, and M. Ronchetti, Phys. Rev. B **28**, 784 (1983).
18) M. D. Rintoul and S. Torquato, J. Chem. Phys. **105**, 9258 (1996).
19) W. Lechner and C. Dellago, J. Chem. Phys. **129**, 114707 (2008).
20) A. Panaitescu, K. A. Reddy, and A. Kudrolli, Phys. Rev. Lett. **108**, 108001 (2012).
21) C. Desgranges and J. Delhommelle, Phys. Rev. B **77**, 054201 (2008).
22) Y. Suzuki, T. Sawada, and K. Tamura, J. Cryst. Growth **318**, 780 (2011).
23) A. Mori, S. Yanagiya, Y. Suzuki, and K. Ito, J. Chem. Phys. **124**, 174507 (2006).